$CoFe_2O_4/TiO_2$-Nb_2O_5 MAGNETIC PHOTOCATALYSTS APPLIED TO CHROMIUM REDUCTION

M.E.K. Fuziki[1], L. S. Ribas[2], E.T.de Paula[2], R. Brackmann[3], O.A.A. dos Santos[1,3], G. G. Lenzi[2]

[1]Departamento de Engenharia Química, Universidade Estadual de Maringá, Maringá, PR, 87020-900, Brazil;
[2]Departamento de Engenharia Química, Universidade Tecnológica Federal do Paraná, Ponta Grossa, PR, 84017-220, Brazil;
[3]Departamento de Química, Universidade Tecnológica Federal do Paraná, Pato Branco, PR, 85503-390, Brazil.
Presenting author email: gianeg@utfpr.edu.br

Abstract

Purpose: Among the heavy metals, chromium stands out, given the high toxicity and carcinogenicity of Cr(VI). The photocatalytic reduction of Cr(VI) has been gaining prominence as an alternative for remediating water contamination. Advances in the use of magnetic photocatalysts have opened up new possibilities for its large-scale application, given the ease of catalyst separation. The present work proposes the preparation of $CoFe_2O_4/TiO_2$-Nb_2O_5 magnetic catalysts and their application in the photocatalytic reduction of chromium. **Methods:** The $CoFe_2O_4/TiO_2$-Nb_2O_5 magnetic catalysts were synthesized by combining cobalt ferrite and TiO_2-Nb_2O_5 through chemical (sol-gel synthesis) or physical mixing (mortar and pestle). The catalysts were characterized by SEM/EDS and XRD applied to the Cr(VI) reduction. Both a synthetic solution and a real effluent were used in the tests. The effects of pH, the addition of hole scavengers, catalyst concentration, and TiO_2-Nb_2O_5 content were evaluated. **Results:** Adding 0.01M sodium formate at pH 2 proved the best Cr(VI) reduction condition. Cobalt ferrite stood out for its ability to remove Cr(VI), but only pure TiO_2-Nb_2O_5 showed considerable capacity to remove total chromium. As for the $CoFe_2O_4/TiO_2$-Nb_2O_5 combination, only the catalyst obtained by physical mixing could remove both Cr(VI) and total chromium. **Conclusions:** The synthesized magnetic catalysts showed promising results for application in actual conditions, with room for studying the reuse of catalysts and the effect of Cr speciation on the photocatalysis process.

Keywords: Heterogeneous photocatalysis, Emerging pollutants, Heavy metals, sol-gel synthesis.

1. Introduction

Given the harmful effects of heavy metals on humans [1,2], plants, and aquatic life [3], there is great interest in improving heavy metal pollution remediation methodologies. Chromium contamination causes considerable concern, given the high toxicity, carcinogenicity, and mobility of the Cr(VI) species in an aqueous environment [4]. Chromium speciation is highly influenced by pH. At basic pH (6.5 – 14), it is found predominantly in the form of chromate (CrO_4^{2-}), followed by hydrogen chromate ($HCrO_4^-$) and dichromate ($Cr_2O_7^{2-}$) in the range between 0.7 and 6.5, and finally in acid chromic ($H_2Cr_2O_7$) at pH less than 0.7 [5]. Cr(III), in turn, forms hexacoordinated complexes at pH between 0 and 4, as hydrolysis products between 4 and 6, and precipitates in the form of $Cr(OH)_{3(s)}$ at pH greater than 6 [5]. The hexavalent form [Cr(VI)] and the trivalent form [Cr(III)] are the most common oxidation states of chromium, the first being highly mutagenic and carcinogenic through exposure by inhalation or contact [4]. It is commonly present in leather tanning processes and the production of paintings, alloys, catalysts, and refractory and corrosion-resistant products [4,6]. The trivalent form causes less concern due to its lower mobility and toxicity and can even be removed relatively easily by precipitation at basic pH levels. It is common to use Cr(III) salts in tanneries to prevent leather rotting by promoting the formation of a protective layer resulting from the complexation reaction of chromium salts with collagen polypeptides [7]. The reduction of Cr(VI) to Cr(III) is an exciting strategy for water treatment [8,9], being one of the possible remediation methodologies, together with membrane filtration, electrochemical precipitation, ion exchange, solvent extraction, and photocatalytic reduction [10]. The possibility of reducing Cr(VI) to Cr(III) by photocatalysis using TiO_2 has already been considerably studied over the years [8,11–13]. Wang et al. (2008) achieved satisfactory results for Cr(VI) reduction and studied the effect of addition of different organics during the photocatalytic process [8]. Testa et al. (2004) also reported exciting results in this sense, achieving complete Cr(VI) reduction in 15 min of irradiation using TiO_2 combined with EDTA in pH 2 and air bubbling [4]. Kumar et al. (2023) proposed the combination of H_2 evolution with simultaneous benzophenone-3 and Cr(VI) removal, using Nb_2O_5/reduced graphene oxide nanocomposite, achieving 87% Cr(VI) reduction [14]. More recently, niobium-based materials have also gained prominence for chromium reduction. Josué et al. (2020), for example, managed to reduce Cr(VI) using non-calcined Nb_2O_5 [15], while Agrafioti et al. (2023) prepared Ti-based films modified with CuO and Nb_2O_5 observing the superior activity of the mixed oxides in photocatalytic reduction of Cr(VI). The author highlighted that the presence of Nb_2O_5 enabled the formation of a Z-scheme in the mixed oxide [16].

The ease of separation of the catalyst has stimulated the use of magnetic photocatalysts, such as that applied by Sin et al. (2022), who achieved simultaneous removal of 4-chlorophenol and Cr(VI) using a magnetic photocatalyst – $CoFe_2O_4$/P-doped BiOBr. In addition to promoting 100% Cr(VI) reduction in 75 min, the photocatalyst proved to be magnetically separable, dispensing the filtration step and maintaining considerable

activity even after five cycles of reuse [17]. Also focused on improving separation/recovery, Ge et al. (2021) applied a magnetic photocatalyst – $Fe_3O_4/FeWO_4$ – achieving almost total removal in 160 min of irradiation [18], while Ibrahim et al. (2020) combined TiO_2 with the magnetic cobalt ferrite, producing $Ag/TiO_2/CoFe_2O_4$ photocatalyst capable of removing more than 90% Cr(VI) in 150 min of UV irradiation [19].

In this context, the present work proposes the use of a $CoFe_2O_4/TiO_2$-Nb_2O_5 magnetic photocatalyst to explore the magnetic properties of cobalt ferrite and the advantages of the TiO_2-Nb_2O_5 combination to improve chromium photocatalytic reduction process. The study encompasses both its application in a synthetic effluent, considering the effect of factors such as $CoFe_2O_4$ and TiO_2-Nb_2O_5 combination method, pH, addition of hole scavenger, proportion between $CoFe_2O_4$ and TiO_2-Nb_2O_5 and catalyst concentration.

2. Materials and Methods

The preparation of magnetic photocatalysts ($CoFe_2O_4/TiO_2$-Nb_2O_5) consisted of two main steps: preparing magnetic cobalt ferrite ($CoFe_2O_4$) and coating/mixing with TiO_2-Nb_2O_5. Cobalt ferrite was prepared using a simple adapted auto-combustion method, while the preparation of $CoFe_2O_4/TiO_2$-Nb_2O_5 was performed through two different strategies that will be presented in the following sections. The catalysts were then characterized by SEM/EDS and applied in photocatalytic reduction of chromium, initially in tests using a synthetic effluent and later applied to a real effluent from a tannery.

2.1 $CoFe_2O_4$ synthesis: auto-combustion methodology

Cobalt ferrite was prepared through a simple adapted auto-combustion method, using $(Co(NO_3)_2.6H_2O$ and $Fe(NO_3)_3.9H_2O$ as precursors. The salts were dissolved in ultrapure water and mixed in a stoichiometric ratio Co:Fe = 1:2. Citric acid (CA) was then added to the solution. The total volume of water used was around 50 mL. The solution was stirred to ensure that it was completely homogeneous, heated to a temperature between 85°C and 90°C to evaporate the water, and the heating was maintained until ignition, which resulted in the formation of a black solid, which was crushed and stored.

2.2 $CoFe_2O_4$ coating with TiO_2-Nb_2O_5: sol-gel methodology

The first approach used to prepare the $CoFe_2O_4/TiO_2$-Nb_2O_5 catalyst was chemical mixing, covering the $CoFe_2O_4$ particles with a layer of TiO_2-Nb_2O_5 using the sol-gel method described in a previous work [20]. To prepare approximately 5g of magnetic photocatalyst, 4g of $CoFe_2O_4$ were weighed and dispersed in isopropanol, and the suspension was sonicated for 1h. Meanwhile, following the methodology described in detail by Fuziki et al. (2023a), $NbCl_5$ and titanium isopropoxide were added to isopropanol in the ratio (Ti+Nb):isopropanol=1:25 and Ti:Nb=75:25, followed by the addition of Tween 20. The solution containing the Ti and Nb precursors was added to the sonicated $CoFe_2O_4$ suspension and vigorously stirred, with the immediate addition of an aqueous solution of NH_4OH (NH_4OH:(Ti+Nb)=1:1, molar basis), dropwise, resulting in instantaneous gel formation. The mixture was stirred for 5 min. At the end, the precipitate was magnetically separated and placed in an oven at 60°C for 12h. The dried material was crushed and calcined at 500°C for 5h, with a heating rate of 1°C/min. The catalyst obtained was named as $CoFe_2O_4/TiO_2$-Nb_2O_5 (chem.).

2.3 $CoFe_2O_4/TiO_2$-Nb_2O_5 preparation: physical mixing

Alternatively, another preparation route was used to obtain the $CoFe_2O_4/TiO_2$-Nb_2O_5 catalyst, which consisted of the physical/mechanical mixture of $CoFe_2O_4$ (prepared as described in section 6.2.2) and TiO_2-Nb_2O_5 (prepared as described by Fuziki et al. (2023b), referring to the 25Nb-1N-400 catalyst). The two oxides were mixed in the proportion $CoFe_2O_4$:TiO_2-Nb_2O_5 = 4:1 and ground intensely in a mortar and pestle for 15 minutes. The catalyst obtained was named $CoFe_2O_4/TiO_2$-Nb_2O_5 (phys.).

2.4 Photocatalysts Characterization

The surface appearance of the catalyst was characterized using scanning electron microscopy (SEM) and energy-dispersive X-ray spectroscopy (EDS) (Tescan Scanning Electron Microscope, Vega 3 LMU equipped with dispersive energy detector—EDS-Oxford, AZTec Energy X-Act). Crystalline phases of the catalysts were identified through X-ray diffraction (XRD) analysis (MiniFlex 600, with Cu Kα radiation, λ = 1.5406 Å) operated at 40 kV and 15 mA.

2.5 Preliminary tests: salicylic acid degradation

The photocatalytic activity of the catalyst was first assessed in salicylic acid (SA) degradation tests at pH 3. The conditions used were similar to those described in [20]. The catalyst (1.0 $g.L^{-1}$) was added to approximately 300 mL of SA solution, 50 $mg.L^{-1}$. The suspension was kept in the dark for 30 minutes until adsorption reached equilibrium, and then a 250 W mercury vapor lamp was activated, starting the photocatalysis stage, which lasted 60 min. Samples were collected at determined times, centrifuged, and stored to determine their concentration by HLPC, as reported in [21]. The tests were conducted at the lowest pH described in [20] to enable comparison with the reported results. Besides, it was considered more relevant to verify the activity of magnetic catalysts at acidic pH, given that some studies demonstrate that an acidic medium is favorable to Cr(VI) reduction (TESTA; GRELA; LITTER, 2004), which is the main objective of the present work.

2.6 Hexavalent chromium reduction: synthetic effluent

In the next stage, Cr(VI) reduction tests were carried out using a synthetic effluent prepared by dissolving potassium dichromate in ultrapure water, with an initial Cr(VI) concentration of 20 $mg.L^{-1}$. The initial

pH of the solution was adjusted to different values (2, 3, 5, and 7) using NaOH and HCl solutions. About 300 mL of Cr(VI) solution was transferred to a temperature-controlled glass reactor under constant stirring. Some tests also included the addition of hole scavengers (formic acid or sodium formate). The catalyst was added (0.5 $g.L^{-1}$), and the suspension was kept in the dark for about 30 minutes. After this interval, the 250W lamp was activated, and the test continued for 60 minutes, with sample collection at determined periods. The samples were collected, centrifuged, and stored to determine the Cr(VI) concentration by UV-Vis spectrophotometry (measurement at 355 nm, Double beam UV-VIS spectrophotometer N6000) and Cr(Total) concentration by atomic absorption spectrometry (AAS, Perkin Elmer AAnalyst 700).

2.7 Preliminary Salicylic Acid Degradation Tests

Initially, the photocatalytic activity of magnetic catalysts was evaluated and compared with the activity of other catalysts tested by Fuziki et al. (2023) through salicylic acid (SA) degradation tests (Figure 1). Since studies have already demonstrated that chromium reduction tends to be favored in acidic conditions, the photocatalytic activity of SA degradation was evaluated at the lowest pH tested in Fuziki et al. (2023) for comparison purposes [20].

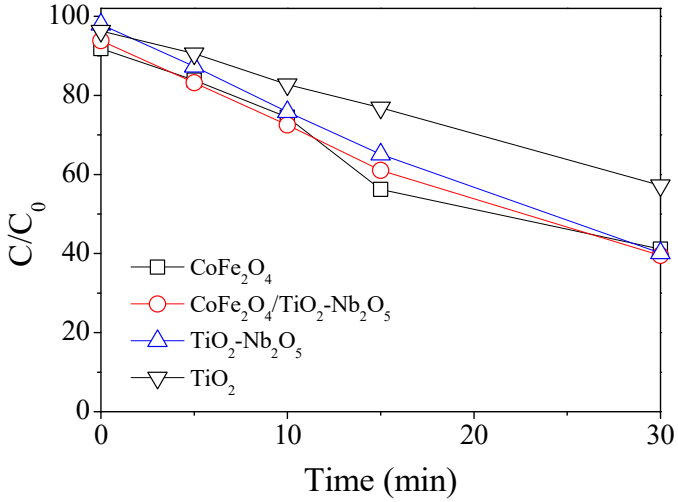

Figure 1 – Salicylic acid photocatalytic degradation tests using different catalysts. Solution pH = 3, catalyst concentration = 1.0 $g.L^{-1}$, $[SA]_0$ = 50 $mg.L^{-1}$, irradiation source = 250 W Hg vapor lamp.

The results (Figure 1) revealed that the cobalt ferrite, the mixed oxide TiO_2-Nb_2O_5, and the combination of both presented similar SA degradation activity, considerably higher than pure TiO_2. Furthermore, the $CoFe_2O_4$ and $CoFe_2O_4$/TiO_2-Nb_2O_5 catalysts showed the capacity for magnetic separation.

Once the photocatalytic activity of the materials was proven, the subsequent testing stage was carried out to reduce chromium in a synthetic effluent.

2.8 $CoFe_2O_4$/TiO_2-Nb_2O_5 Photocatalysts Applied to Chromium Reduction – Synthetic Effluent Tests Overview

The following sections present the results of chromium reduction tests using a chromium solution prepared from chromium dichromate salt, simulating an effluent. The initial experiments were carried out using the $CoFe_2O_4$/TiO_2-Nb_2O_5 magnetic catalyst prepared through the chemical mixture of $CoFe_2O_4$ and TiO_2-Nb_2O_5, i.e., $CoFe_2O_4$ coating with TiO_2-Nb_2O_5 by a sol-gel methodology. The initial tests aimed to adjust the best pH, determine whether or not to use a hole scavenger and its concentration, and determine the best catalyst concentration. Furthermore, the contribution of photolysis to the process was also considered, and the performance of the pure components was compared ($CoFe_2O_4$ and TiO_2-Nb_2O_5). For further analysis, not only the Cr(VI) concentration by UV-Vis spectroscopy was monitored, but also the total Cr concentration by AAS measurements.

2.9 Effects of solution pH and hole scavenger addition

In the tests considering different solution pHs (3, 5, and 7, Figure 2a), it was only possible to notice the reduction of Cr(VI) in the test carried out at pH 3, with practically no removal at pH 5 and 7. Although pH 3 has already been proven sufficient to promote Cr(VI) reduction, another test was carried out at pH 2, as this value had already been extensively reported in other studies [4,8,15]. In pH 2, a discrete improvement was observed compared to pH 3, reaching a 4.5% reduction in 60 minutes of irradiation. According to Cappelletti et al. (2008), at pH 2.5, the effect of dissolved O_2 is negligible. Therefore, pH 2 was chosen to ensure that the presence of O_2 would not affect the tests performed [9]. Furthermore, studies for TiO_2 and Nb_2O_5 have already indicated that pH 2 is the best for reducing Cr(VI). For example, Testa et al. (2004) achieved better chromium reduction results at pH 2 compared to pH 3 using TiO_2 [4]. Joshua et al. also reported better results at pH 2 using either calcined or not calcined Nb_2O_5 [15].

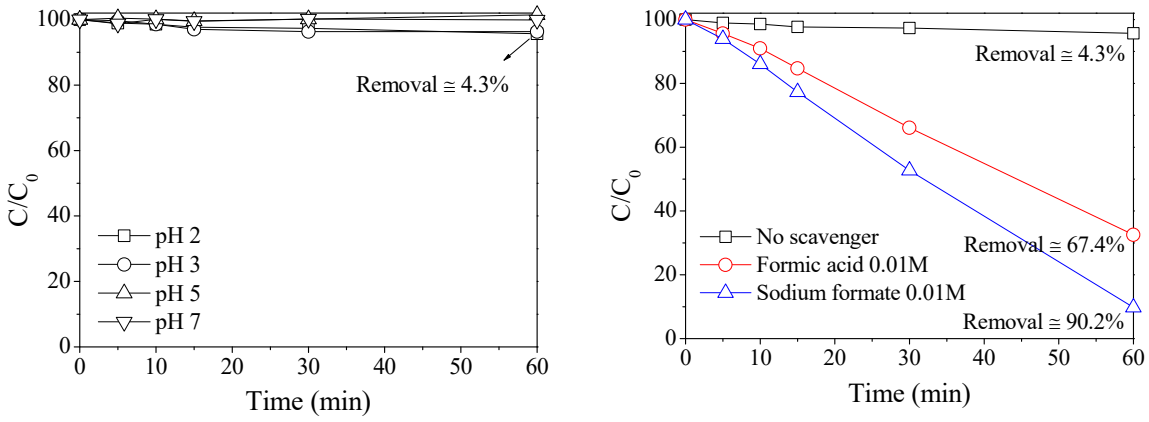

Figure 2 – Photocatalytic reduction of Cr(VI) using $CoFe_2O_4/TiO_2$-Nb_2O_5 photocatalyst (chem., sol-gel) (a) at different pH with no hole scavenger and (b) with and without the use of hole scavengers at pH 2. $[Cr(VI)]_0$ = 20 $mg.L^{-1}$, photocatalyst concentration = 0.5 $g.L^{-1}$.

The positive effect observed for the pH reduction (Figure 2a) reflects both the increase in the driving force of electron transfer with the decrease in pH related to the Cr(VI)/Cr(III) reduction potentials and the conduction band potential of the catalyst, as well as the increased electrostatic attraction between the catalyst surface and the anionic form of Cr(VI) at lower pH [9].

The second test evaluated the effects of adding two organic compounds to act as hole scavengers. The beneficial effects of adding organic molecules during the reduction of Cr(VI) were already recognized for different compounds, given their scavenging action on photogenerated holes, reducing the recombination of e^-/h^+ pairs [8]. Presently, two hole scavengers were evaluated: formic acid and sodium formate. Formic acid's hole scavenger action is already well known for chromium [8,9] and also for other heavy metals, such as lead [22] and selenium [23]. It has advantages over other electron donors, such as isopropanol, as it does not introduce toxic compounds into the medium due to its degradation [22]. For some metals such as cadmium, lead, and selenium, sodium formate showed excellent results, and in some cases, it was superior to formic acid itself[24–26].

The results (Figure 2b) showed that adding hole scavengers improved chromium reduction, with sodium formate showing the best performance. In addition to the evident improvement in Cr(VI) removal, sodium formate did not cause a significant change in the pH of the solution, which was considered an advantage. Once sodium formate (SF) was selected as the hole scavenger to be used, tests were carried out with three different concentrations of SF (0.1M, 0.01M, and 0.001M, Figure 3)

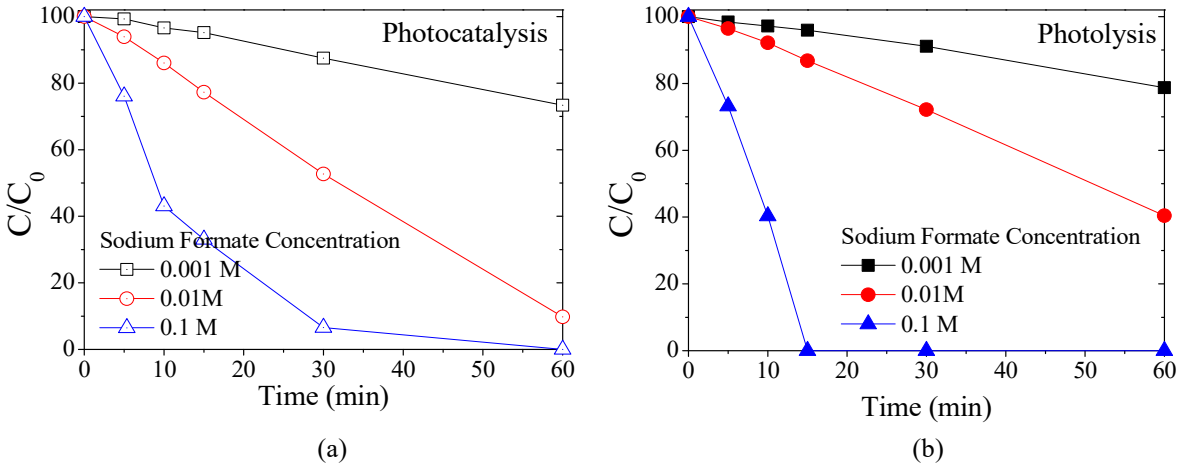

Figure 3 – (a) Photocatalytic reduction of Cr(VI) using $CoFe_2O_4/TiO_2$-Nb_2O_5 (chem., sol-gel) at different sodium formate concentrations: pH=2; $[Cr(VI)]_0$ = 20 $mg.L^{-1}$, photocatalyst concentration = 0.5 $g.L^{-1}$; (b) Photolysis of Cr(VI) at pH 2 using different sodium formate concentrations.

Photocatalytic tests (Figure 3a) showed that increasing the SF concentration resulted in greater Cr(VI) removal in 60 minutes of irradiation. When the concentration increased from 0.001M to 0.01M, removal was substantially improved, which went from around 26.6% to more than 90% at the end of the test. When the concentration was increased from 0.01M to 0.1M, the improvement in removal was less intense, which was more evident at the beginning of the test, even though there was a 10-fold increase in the SF concentration. The increased Cr(VI) removal with increasing sodium formate concentration indicates no competitive adsorption effect between the pollutant and formate ions, which could harm the process [25]. On the contrary, increasing removal with

increasing hole scavenger concentration suggests sodium formate contributes to Cr(VI) reduction by preventing the recombination of electron-hole pairs or the action of radicals formed during its degradation [9].

Tests were also carried out with different concentrations of SF but without adding a photocatalyst (Figure 3b) to evaluate photolysis contribution. The results revealed that only the presence of SF combined with UV radiation can promote the reduction of Cr(VI). Given that no catalyst was present in the medium, the action of sodium formate is not restricted to the hole scavenger effect, as photogeneration of holes does not occur. Thus, it is concluded that the formation of radicals from the photolysis or photocatalysis of sodium formate plays a vital role in the reduction of chromium, similar to what was observed by Cappelletti et al. (2008) regarding isopropanol [9].

When comparing the results of photolysis (Figure 3b) and photocatalysis (Figure 3a), it is possible to observe the improvement in the reduction of Cr(VI) with the addition of the photocatalyst for concentrations 0.001M and 0.01M of SF, being more evident in the latter case. For the concentration of 0.1M SF, on the other hand, the addition of the catalyst seems to have a negative effect on the removal, most likely due to the catalyst's dark color, limiting the incidence of radiation in the suspension.

2.10 Total chromium – Cr(Total) – removal

The total concentration of Cr present in the solution was determined using AAS to complement the analysis of the results. The results, shown in Figure 4, revealed that the total chromium removal was almost negligible in the case of photolysis with 0.1M SF (Figure 4a). Interestingly, even the magnetic catalyst was not able to promote a considerable removal of Cr(Total), with only a tiny decrease in concentration in the early stages of the test (Figure 4b), most likely caused by the adsorption of Cr(VI).

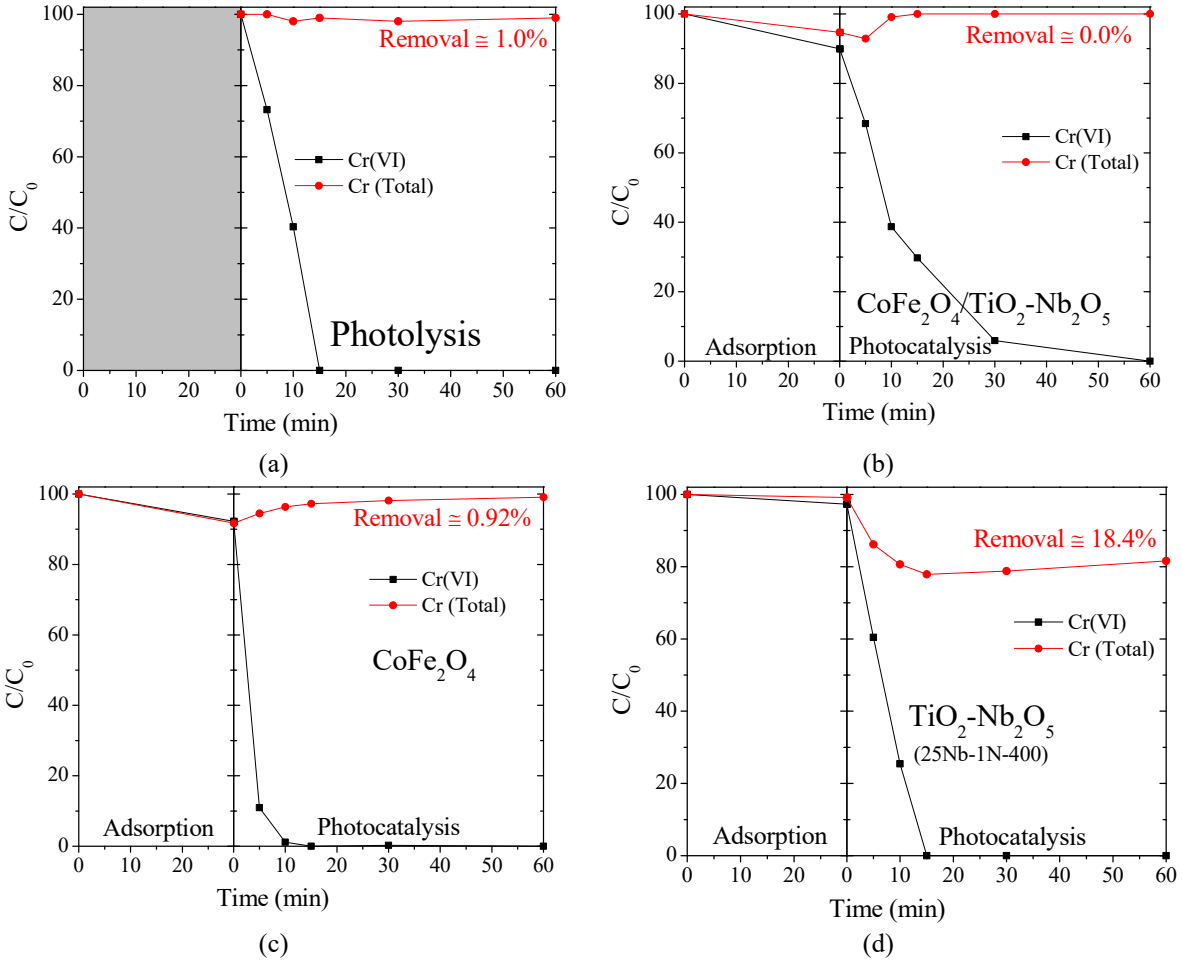

Figure 4 – Photocatalytic reduction of Cr(VI) (black) and total Cr (red) using different photocatalysts. Comparison between (a) photolysis and photocatalysis (b-d) using as photocatalysts: (b) cobalt ferrite coated with TiO_2-Nb_2O_5, (chem., sol-gel) (c) bare cobalt ferrite and (d) TiO_2-Nb_2O_5. [Cr(VI)]0 = 20 mg.L-1, photocatalyst concentration = 0.5 g.L-1, pH = 2, [sodium formate] = 0.1 M.

Additional tests were carried out separately in the same condition with cobalt ferrite and TiO_2-Nb_2O_5. Cobalt ferrite (Figure 4c) stood out for its remarkable ability to reduce Cr(VI), reaching around 90% removal in just 5 minutes of irradiation. Despite the considerable adsorption of chromium, it could not promote total

chromium removal after 60 minutes of irradiation. TiO_2-Nb_2O_5 (Figure 4d), on the other hand, showed considerable Cr(VI) removal, very similar to that of photolysis under the same conditions, but was able to promote around 18% Cr(Total) removal in 60 minutes of irradiation. Similar tests were then carried out at a concentration of 0.01M SF (Figure 5).

Again, photolysis was unable to remove total chromium. Furthermore, for a concentration of 0.01M SF, all three catalysts tested showed higher percentages of Cr(VI) removal than that obtained in the photolysis test, proving their photocatalytic activity and contribution to Cr(VI) reduction. Under such conditions, pure and TiO_2-Nb_2O_5 coated $CoFe_2O_4$ slightly removed about 4.5% of Cr(Total). In comparison, pure TiO_2-Nb_2O_5 removed 18.7% of Cr(Total), even with a 10-fold decrease in SF concentration compared to previous tests (Figure 4). For these reasons, it was decided to set the SF concentration in the following tests as 0.01M.

Regarding the removal of total chromium, TiO_2-Nb_2O_5 stands out. Both TiO_2 and Nb_2O_5 separately (Figure 6) are capable of promoting a considerable reduction of Cr(VI) (79.9% and 77.9%, respectively), with their combination being slightly more efficient in this process. In comparing the oxides, TiO_2 was the main responsible for removing Cr (Total), reaching almost 24% removal in 60 min. The TiO_2-Nb_2O_5 combination slightly improved the percentage of Cr(VI) reduction (85.9%, Figure 3) without a significant loss of total chromium removal capacity.

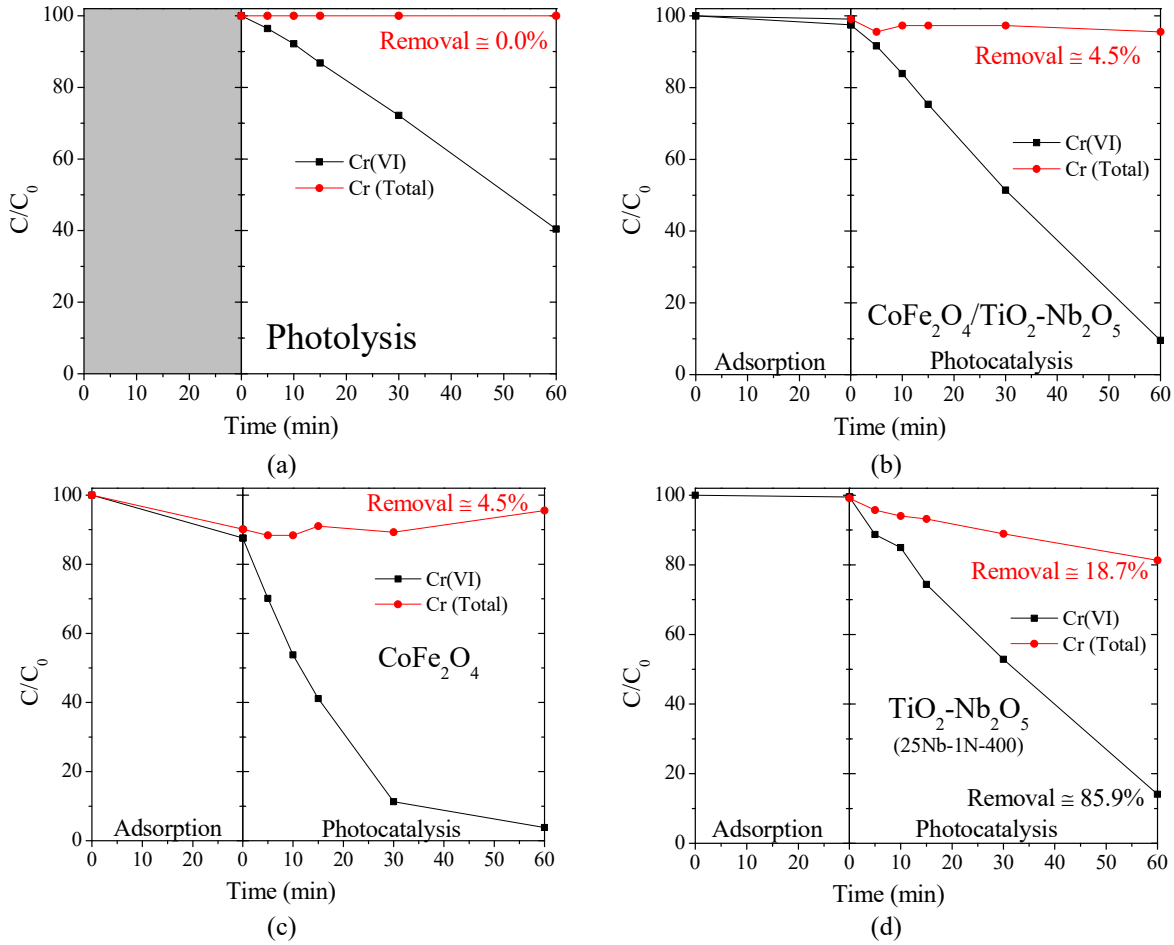

Figure 5 – Photocatalytic reduction of Cr(VI) (black) and total Cr (red) using different photocatalysts. Comparison between (a) photolysis and photocatalysis (b-d) using as photocatalysts: (b) cobalt ferrite coated with TiO_2-Nb_2O_5 (sol-gel) (c) bare cobalt ferrite and (d) TiO_2-Nb_2O_5. $[Cr(VI)]_0$ = 20 $mg.L^{-1}$, photocatalyst concentration = 0.5 $g.L^{-1}$, pH = 2, [sodium formate] = 0.01 M.

2.11 Effect of TiO_2-Nb_2O_5 content and catalyst concentration

The results obtained showed the excellent performance of the TiO_2-Nb_2O_5 catalyst in removing both Cr(VI) and Cr(Total), achieving a considerable removal percentage of the latter, unlike that obtained by either pure $CoFe_2O_4$ or $CoFe_2O_4$/TiO_2-Nb_2O_5. Taking this into account and given that the $CoFe_2O_4$/TiO_2-Nb_2O_5 magnetic catalyst contains around 20% TiO_2-Nb_2O_5 in its composition (estimated by the synthesis stoichiometry), the reduced performance of $CoFe_2O_4$/TiO_2-Nb_2O_5 compared to pure TiO_2-Nb_2O_5 is not entirely unexpected.

From these results, two possible approaches were outlined to improve the performance of the $CoFe_2O_4/TiO_2$-Nb_2O_5 magnetic catalyst: increasing the proportion between $CoFe_2O_4$ and the TiO_2-Nb_2O_5 coating or increasing the concentration of $CoFe_2O_4/TiO_2$-Nb_2O_5 in the suspension, to compensate for the lower content of TiO_2-Nb_2O_5 in the photocatalyst. The tests carried out based on these two strategies are presented in Figure 7.

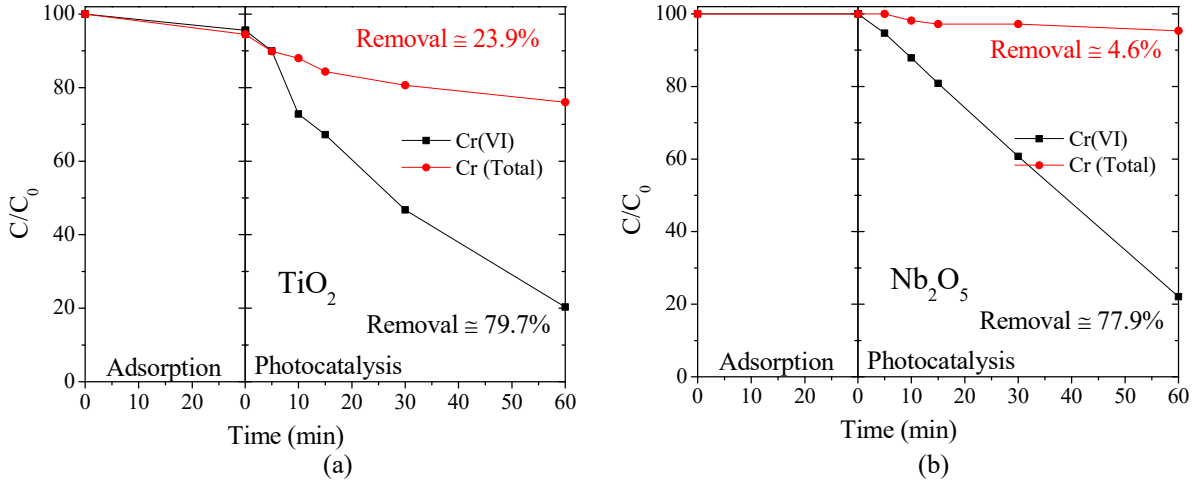

Figure 6 – Photocatalytic reduction of Cr(VI) and total Cr using as photocatalyst: (a) TiO_2 and (b) Nb_2O_5. pH=2; $[Cr(VI)]_0$ = 20 mg.L^{-1}, photocatalyst concentration = 0.5 g.L^{-1}; [sodium formate] = 0.01 M.

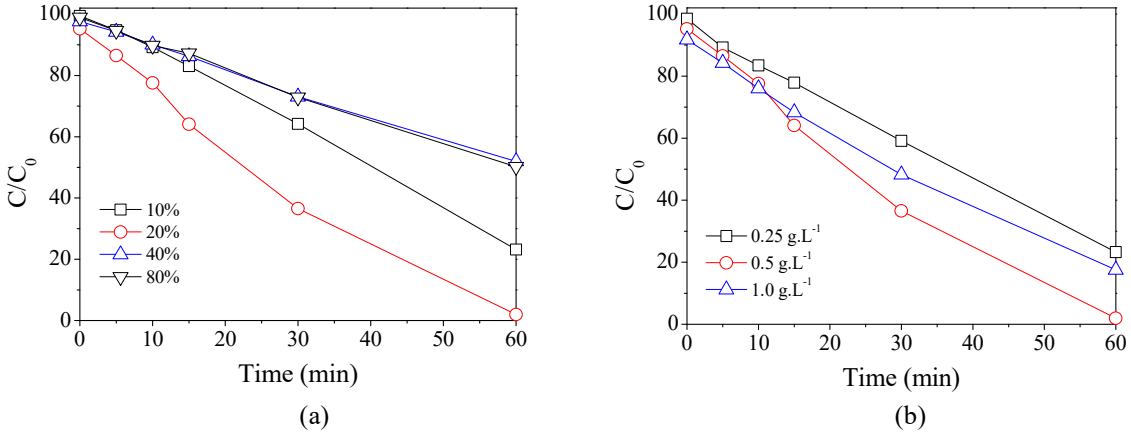

Figure 7 – Photocatalytic reduction of Cr(VI) using $CoFe_2O_4/TiO_2$-Nb_2O_5 (chem., sol-gel) with (a) different nominal TiO_2-Nb_2O_5 coating percentages (from 10% to 80%) and (b) using different concentrations of photocatalyst ($CoFe_2O_4/TiO_2$-Nb_2O_5 – sol-gel), ranging from 0.25 g.L^{-1} to 1.0 g.L^{-1}. pH=2; $[Cr(VI)]_0$ = 20 mg.L^{-1}, photocatalyst concentration = 0.5 g.L^{-1} (when not otherwise indicated); [sodium formate] = 0.01 M.

Figure 7 presents the results for Cr(VI) reduction. As can be seen in the graph in Figure 7a, increasing TiO_2-Nb_2O_5 content from 10% to 20% led to an improvement in the Cr(VI) removal. However, increasing TiO_2-Nb_2O_5 content above 20% led to a decrease in Cr(VI) reduction. Regarding the total chromium concentration, no removal was observed for the magnetic catalyst containing 10% of TiO_2-Nb_2O_5. In comparison, for 20% and 40% of TiO_2-Nb_2O_5, the removal achieved 4.5% and 7.2% in 60 min, respectively (results not shown in the figures). However, increasing the TiO_2-Nb_2O_5 content to 80% resulted in no total chromium removal. Additionally, a significant drop in the magnetic properties of the photocatalysts was observed as the TiO_2-Nb_2O_5 content increased. Based on these results, the catalyst containing 20%TiO_2-Nb_2O_5 was chosen to continue the tests, as it combined the best performance in removing Cr(VI) and Cr(Total) and reasonable magnetic properties.

Considering the magnetic catalyst with 20% TiO_2-Nb_2O_5, tests were conducted at different catalyst concentrations (0.25, 0.5, and 1.0 g.L^{-1}, Figure 7b). A diminished removal of Cr(VI) was observed at both the lowest and the highest catalyst concentrations (0.25 g.L^{-1} and 1.0 g.L^{-1}). The best result was obtained for the intermediate value of 0.5 g.L-1. The decrease in removal with increased catalyst mass to a value larger than 0.5 g.L^{-1} was contrary to what could be expected at first. The excessive mass of the catalyst probably became harmful to the incidence of radiation in the suspension.

2.12 Photocatalyst characterization: SEM/EDS Results

This section presents the SEM/EDS characterization results. Although this is a semi-quantitative analysis, the estimates of the concentrations of the elements on the catalyst surface allowed a better understanding of the possible causes of the results obtained in the photocatalytic tests. Analysis of pure cobalt ferrite (Figure 8) and pure TiO_2-Nb_2O_5 (Figure 9) indicated a reasonably homogeneous distribution of elements. Both exhibited a wide range of particle sizes (with smaller sizes in cobalt ferrite, as seen in Figure 8a), with shard-like shapes.

Considering the stoichiometry of the oxides and the molar mass of the elements, the estimated composition of $CoFe_2O_4$ would be around 25.1% Co, 47.6% Fe, and 27.3% O, which is in reasonable agreement with the values estimated by EDS (28.4 %, 45.8% e 25.8% for Co, Fe, and O, respectively). As for TiO_2-Nb_2O_5, the stoichiometry indicated a composition of 34.8% of Ti, 22.5% of Nb, and 42.7% of O, in good agreement with the EDS semi-quantitative estimation of 36.6% of Ti, 20.8% of Nb and 42.5% of O (Figure 9b).

In the case of the $CoFe_2O_4$/TiO_2-Nb_2O_5 magnetic photocatalyst, some divergences can be observed between the stoichiometric estimates and the EDS estimates (Table 1 and Figure 10b). Furthermore, the distribution maps of each element (Figure 10c to 10g) indicated that Ti and Nb are not present homogeneously across the catalyst particles, i.e., the coating with TiO_2-Nb_2O_5 did not occur equally on the particles. Spot analyses carried out at some random sample points (Figure 11) highlight the large discrepancy in the distribution of elements on the catalyst surface.

Table 1 – Stoichiometric and EDS elemental composition estimations for $CoFe_2O_4$/TiO_2-Nb_2O_5 catalyst

	Co	Fe	O	Ti	Nb
Stoichiometry	20.1 %	38.1%	30.3%	7.0%	4.5%
EDS estimation	22.2%	37.0%	26.2%	7.7%	7.0%

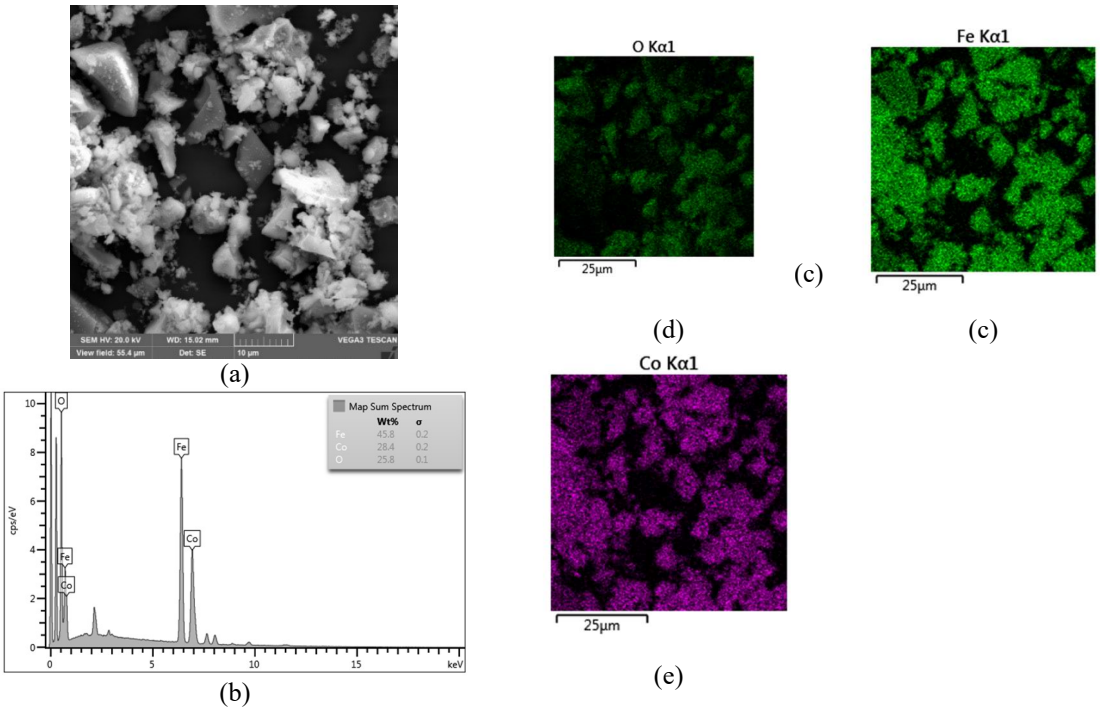

Figure 8 – MED/EDS results: (a) MEV image of $CoFe_2O_4$, (b) EDS spectrum, and (c-e) elemental distribution.

Furthermore, the EDS estimates indicated a higher ratio of Nb to Ti than would be expected from stoichiometry or what was observed by EDS estimation for the pure TiO_2-Nb_2O_5 sample. Although other characterizations are necessary for a conclusive analysis, the SEM/EDS results suggest that the formation of the TiO_2-Nb_2O_5 layer on $CoFe_2O_4$ does not occur in the same way as in the pure TiO_2-Nb_2O_5 synthesis process, and therefore, this layer would not have a constitution and characteristics similar to pure TiO_2-Nb_2O_5, and consequently, not the same photocatalytic activity.

The presence of $CoFe_2O_4$ particles during the TiO_2-Nb_2O_5 sol-gel synthesis seems to interfere with the hydrolysis and condensation kinetics, favoring the Nb deposition. XRD results (Figure 12) led to similar conclusions.

While for the pure TiO_2-Nb_2O_5 catalyst calcined at 400°C it was possible to identify the predominance of the Anatase (PDF #71-1167) and TT-Nb_2O_5 (PDF# 28-0317) phases, for the $CoFe_2O_4$/TiO_2-Nb_2O_5 magnetic catalysts the formation of the rutile phase (PDF#78-1510) was favored and it is not possible to detect characteristic peaks for niobium phases (Figure 12 b-e). The increase in the rutile content in magnetic catalysts could be mainly responsible for the decreased photocatalytic activity, given that some studies suggest the lower activity of the rutile phase compared to anatase for some processes [27]. Also noteworthy is the increase in crystallinity of the $CoFe_2O_4$ phase after calcination at 400 °C, as seen in the mixed samples. For very high levels of TiO_2-Nb_2O_5, a considerable reduction in the sample's crystallinity was observed.

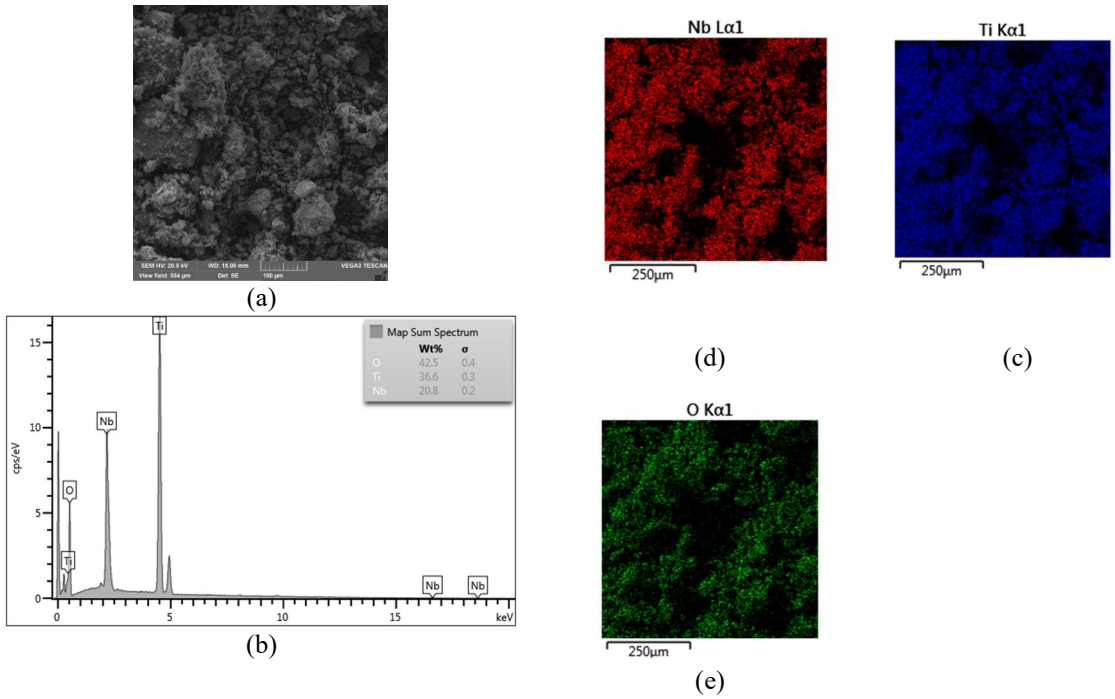

Figure 9 – MED/EDS results: (a) MEV image of TiO_2-Nb_2O_5 (b) EDS spectrum and (c-e) elemental distribution.

The characterization and photocatalytic test results suggest that the sol-gel methodology was unsuitable for combining $CoFe_2O_4$ and TiO_2-Nb_2O_5 while preserving the individual characteristics of the oxides. As an alternative, the production of $CoFe_2O_4$/TiO_2-Nb_2O_5 was carried out through a simple physical/mechanical mixing process using a mortar and pestle.

The obtained magnetic catalyst was tested for chromium reduction (Figure 13a) and exhibited good performance, reaching 92.7% Cr(VI) removal and 17.7% Cr(Total) removal in 60 min of irradiation. In Figure 13b, it is possible to observe the result obtained by the magnetic catalyst prepared by physical mixing – $CoFe_2O_4$/TiO_2-Nb_2O_5 (phys.) – in comparison to the results of the magnetic catalyst obtained by chemical mixing (sol-gel methodology) – $CoFe_2O_4$/TiO_2-Nb_2O_5 (chem.) – and pure TiO_2-Nb_2O_5. The catalyst's performance in reducing Cr(VI) is drastically superior to that of the other two photocatalysts, and its removal of Cr(Total) is comparable to that of pure TiO_2-Nb_2O_5, making it chosen as the best photocatalyst for the next steps.

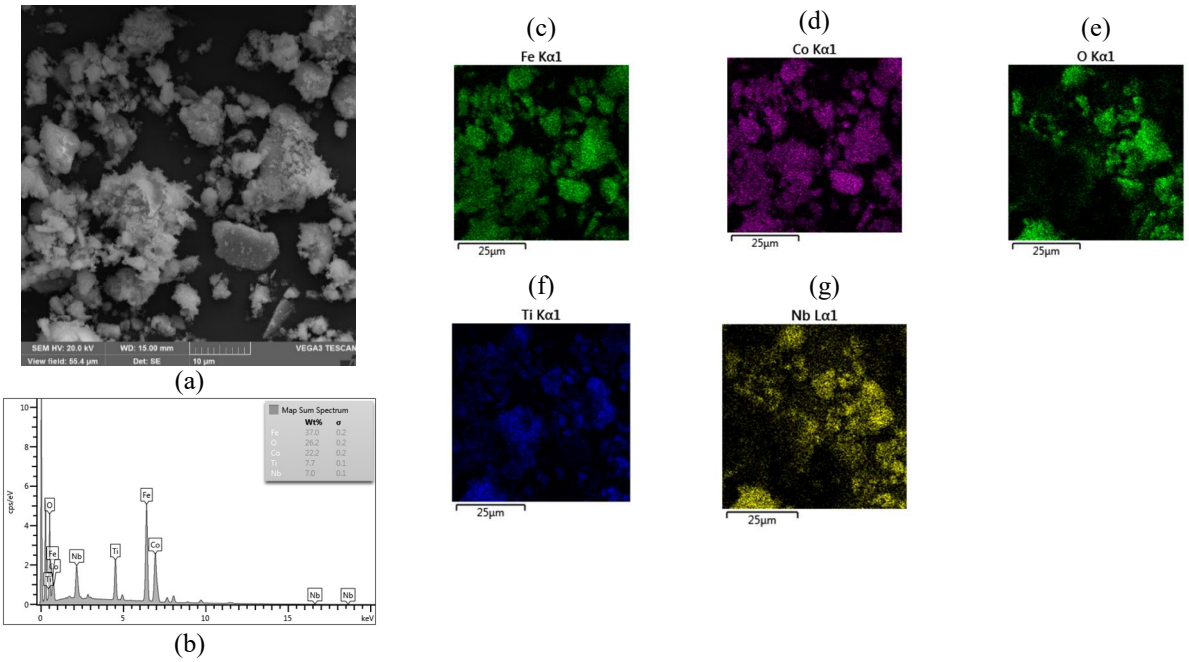

Figure 10 – MED/EDS results: (a) MEV image of $CoFe_2O_4/TiO_2$-Nb_2O_5, (b) EDS spectrum, and (c-g) elemental distribution.

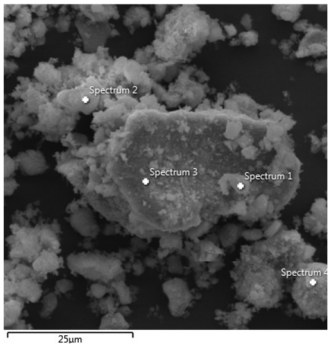

	Element (%)				
Spectrum	**Fe**	**Co**	**O**	**Nb**	**Ti**
1	41.4	22.8	29.2	5.0	1.6
2	38.3	21.1	31.5	6.7	2.4
3	49.0	29.0	17.9	3.6	0.5
4	20.3	13.3	43.9	11.5	11.0

Figure 11 – EDS spectra of different spots on the $CoFe_2O_4/TiO_2$-Nb_2O_5 sample.

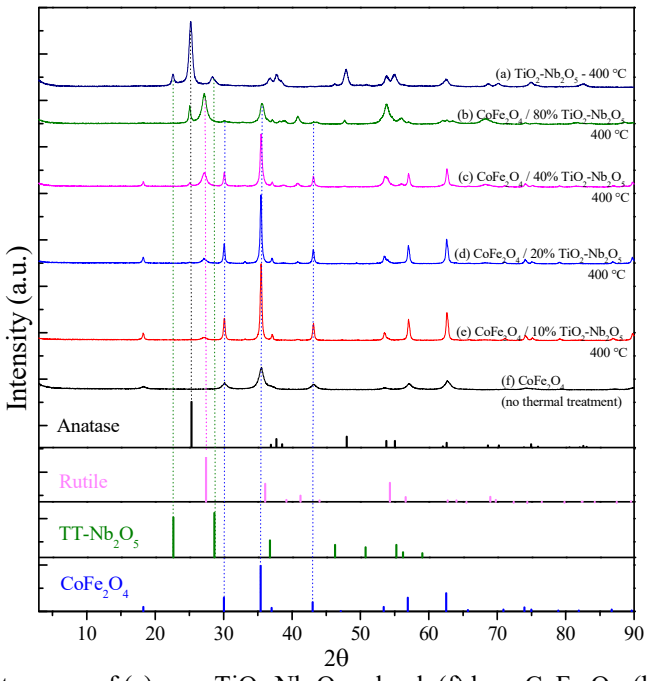

Figure 12 – X-ray diffractograms of (a) pure TiO_2-Nb_2O_5 sol-gel, (f) bare $CoFe_2O_4$, (b-e) and magnetic catalysts with different TiO_2-Nb_2O_5 content.

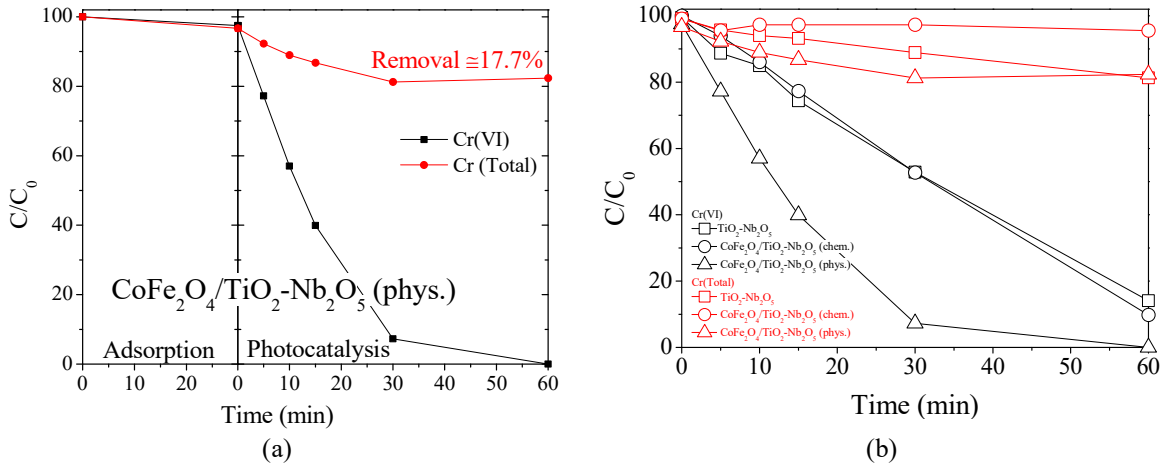

Figure 13 – Photocatalytic reduction of Cr(VI) (black) and total Cr (red) using (a) $CoFe_2O_4/TiO_2$-Nb_2O_5 magnetic photocatalyst obtained through physical mixture. In (b) a performance comparison between $CoFe_2O_4/TiO_2$-Nb_2O_5 (phys.), $CoFe_2O_4/TiO_2$-Nb_2O_5 (chem.) and TiO_2-Nb_2O_5 photocatalysts are presented. $[Cr(VI)]_0$ = 20 $mg.L^{-1}$, photocatalyst concentration = 0.5 $g.L^{-1}$, pH = 2, [sodium formate] = 0.01 M.

3. Conclusions

The results currently obtained are promising for applying magnetic catalysts to real effluents. TiO_2-Nb_2O_5 modified with NH_4OH was combined with $CoFe_2O_4$ through a chemical mixture (coating the $CoFe_2O_4$ using sol-gel methodology) and a physical mixture (mixing the oxides in a mortar and pestle) for comparison. Photolysis tests indicated that adding sodium formate, even without a catalyst, is enough to promote the reduction of Cr(VI), with no significant impact on total chromium concentration. In comparing $CoFe_2O_4$ and TiO_2-Nb_2O_5, the first was the most active in reducing Cr(VI) without removing total chromium. At the same time, the second was considerably active in removing both the hexavalent form and total chromium. The magnetic catalyst obtained by physically mixing the oxides proved to be quite active in reducing Cr(VI), the most toxic form of chromium, and reasonably active in removing total chromium from the synthetic effluent.

4. References

1. Li, B.; Xia, M.; Zorec, R.; Parpura, V.; Verkhratsky, A. Astrocytes in Heavy Metal Neurotoxicity and Neurodegeneration. Brain Res 1752, 147234, (2021), doi:10.1016/j.brainres.2020.147234.
2. Renu, K.; Chakraborty, R.; Myakala, H.; Koti, R.; Famurewa, A.C.; Madhyastha, H.; Vellingiri, B.; George, A.; Valsala Gopalakrishnan, A. Molecular Mechanism of Heavy Metals (Lead, Chromium, Arsenic, Mercury, Nickel and Cadmium) - Induced Hepatotoxicity – A Review. Chemosphere 271, 129735, (2021), doi:10.1016/j.chemosphere.2021.129735.
3. Gusso-Choueri, P.K.; Araújo, G.S. de; Cruz, A.C.F.; Stremel, T.R. de O.; Campos, S.X. de; Abessa, D.M. de S.; Oliveira Ribeiro, C.A. de; Choueri, R.B. Metals and Arsenic in Fish from a Ramsar Site under Past and Present Human Pressures: Consumption Risk Factors to the Local Population. Science of the Total Environment 628–629, 621–630, (2018), doi:10.1016/j.scitotenv.2018.02.005.
4. Testa, J.J.; Grela, M.A.; Litter, M.I. Heterogeneous Photocatalytic Reduction of Chromium(VI) over TiO 2 Particles in the Presence of Oxalate: Involvement of Cr(V) Species. Environ Sci Technol 38, 1589–1594, (2004), doi:10.1021/es0346532.
5. Unceta, N.; Séby, F.; Malherbe, J.; Donard, O.F.X. Chromium Speciation in Solid Matrices and Regulation: A Review. *Anal Bioanal Chem* (2010), *397*, 1097–1111.
6. Fournier-Salaün, M.C.; Salaün, P. Quantitative Determination of Hexavalent Chromium in Aqueous Solutions by UV-Vis Spectrophotometer. Central European Journal of Chemistry 5, 1084–1093, (2007), doi:10.2478/s11532-007-0038-4.
7. Fabianil, C.; Rusciol, F.; Spadonil, M.; Pizzichini2, M. *Chromium(III) Salts Recovery Process from Tannery Wastewaters*; (1996); Vol. 108;.
8. Wang, L.; Wang, N.; Zhu, L.; Yu, H.; Tang, H. Photocatalytic Reduction of Cr(VI) over Different TiO2 Photocatalysts and the Effects of Dissolved Organic Species. J Hazard Mater 152, 93–99, (2008), doi:10.1016/j.jhazmat.2007.06.063.
9. Cappelletti, G.; Bianchi, C.L.; Ardizzone, S. Nano-Titania Assisted Photoreduction of Cr(VI). The Role of the Different TiO2 Polymorphs. Appl Catal B 78, 193–201, (2008), doi:10.1016/j.apcatb.2007.09.022.

10. Bashir, M.S.; Ramzan, N.; Najam, T.; Abbas, G.; Gu, X.; Arif, M.; Qasim, M.; Bashir, H.; Shah, S.S.A.; Sillanpää, M. Metallic Nanoparticles for Catalytic Reduction of Toxic Hexavalent Chromium from Aqueous Medium: A State-of-the-Art Review. *Science of the Total Environment* (2022), *829*.
11. Acharya, R.; Naik, B.; Parida, K. Cr(VI) Remediation from Aqueous Environment through Modified-TiO2-Mediated Photocatalytic Reduction. *Beilstein Journal of Nanotechnology* (2018), *9*, 1448–1470.
12. Litter, M.I. Last Advances on TiO2-Photocatalytic Removal of Chromium, Uranium and Arsenic. *Curr Opin Green Sustain Chem* (2017), *6*, 150–158.
13. Islam, J.B.; Furukawa, M.; Tateishi, I.; Katsumata, H.; Kaneco, S. Photocatalytic Reduction of Hexavalent Chromium with Nanosized TiO2 in Presence of Formic Acid. ChemEngineering 3, 1–10, (2019), doi:10.3390/chemengineering3020033.
14. Kumar, K.Y.; Prashanth, M.K.; Shanavaz, H.; Parashuram, L.; Alharti, F.A.; Jeon, B.H.; Raghu, M.S. Green and Facile Synthesis of Strontium Doped Nb2O5/RGO Photocatalyst: Efficacy towards H2 Evolution, Benzophenone-3 Degradation and Cr(VI) Reduction. Catal Commun 173, (2023), doi:10.1016/j.catcom.2022.106560.
15. Josué, T.G.; Almeida, L.N.B.; Lopes, M.F.; Santos, O.A.A.; Lenzi, G.G. Cr (VI) Reduction by Photocatalyic Process: Nb2O5 an Alternative Catalyst. J Environ Manage 268, (2020), doi:10.1016/j.jenvman.2020.110711.
16. Agrafioti, K.A.; Panagiotopoulos, N.T.; Moularas, C.; Deligiannakis, Y.; Prouskas, C.; Soukouli, P.P.; Evangelakis, G.A. Development of Ti-Based Nanocomposite Oxide Thin Films with CuO and Nb2O5 Additions Suitable for Catalytic Applications. Thin Solid Films 775, (2023), doi:10.1016/j.tsf.2023.139864.
17. Sin, J.C.; Lam, S.M.; Zeng, H.; Lin, H.; Li, H.; Huang, L.; Tham, K.O.; Mohamed, A.R.; Lim, J.W. Enhanced Synchronous Photocatalytic 4-Chlorophenol Degradation and Cr(VI) Reduction by Novel Magnetic Separable Visible-Light-Driven Z-Scheme CoFe2O4/P-Doped BiOBr Heterojunction Nanocomposites. Environ Res 212, (2022), doi:10.1016/j.envres.2022.113394.
18. Ge, T.; Jiang, Z.; Shen, L.; Li, J.; Lu, Z.; Zhang, Y.; Wang, F. Synthesis and Application of Fe3O4/FeWO4 Composite as an Efficient and Magnetically Recoverable Visible Light-Driven Photocatalyst for the Reduction of Cr(VI). Sep Purif Technol 263, (2021), doi:10.1016/j.seppur.2021.118401.
19. Ibrahim, I.; Kaltzoglou, A.; Athanasekou, C.; Katsaros, F.; Devlin, E.; Kontos, A.G.; Ioannidis, N.; Perraki, M.; Tsakiridis, P.; Sygellou, L.; et al. Magnetically Separable TiO2/CoFe2O4/Ag Nanocomposites for the Photocatalytic Reduction of Hexavalent Chromium Pollutant under UV and Artificial Solar Light. Chemical Engineering Journal 381, (2020), doi:10.1016/j.cej.2019.122730.
20. Fuziki, M.E.K.; Ribas, L.S.; Abreu, E.; Fernandes, L.; dos Santos, O.A.A.; Brackmann, R.; de Tuesta, J.L.D.; Tusset, A.M.; Lenzi, G.G. N-Doped TiO2-Nb2O5 Sol–Gel Catalysts: Synthesis, Characterization, Adsorption Capacity, Photocatalytic and Antioxidant Activity. Catalysts 13, (2023), doi:10.3390/catal13091233.
21. Fuziki, M.E.K.; Ribas, L.S.; Tusset, A.M.; Brackmann, R.; Dos Santos, O.A.A.; Lenzi, G.G. Pharmaceutical Compounds Photolysis: PH Influence. Heliyon 9, (2023), doi:10.1016/j.heliyon.2023.e13678.
22. Murruni, L.; Conde, F.; Leyva, G.; Litter, M.I. Photocatalytic Reduction of Pb(II) over TiO_2: New Insights on the Effect of Different Electron Donors. Appl Catal B 84, 563–569, (2008), doi:10.1016/j.apcatb.2008.05.012.
23. Holmes, A.B.; Ngan, A.; Ye, J.; Gu, F. Selective Photocatalytic Reduction of Selenate over TiO2 in the Presence of Nitrate and Sulfate in Mine-Impacted Water. Chemosphere 287, 131951, (2021), doi:10.1016/j.chemosphere.2021.131951.
24. Mishra, T.; Hait, J.; Aman, N.; Jana, R.K.; Chakravarty, S. Effect of UV and Visible Light on Photocatalytic Reduction of Lead and Cadmium over Titania Based Binary Oxide Materials. J Colloid Interface Sci 316, 80–84, (2007), doi:10.1016/j.jcis.2007.08.037.
25. Tan, T.T.Y.; Beydoun, D.; Amal, R. Photocatalytic Reduction of Se(VI) in Aqueous Solutions in UV/TiO2 System: Importance of Optimum Ratio of Reactants on TiO2 Surface. J Mol Catal A Chem 202, 73–85, (2003), doi:10.1016/S1381-1169(03)00205-X.
26. Nguyen, V.N.H.; Amal, R.; Beydoun, D.; Nu Hoai Nguyen, V.; Amal, R.; Beydoun, D. Photocatalytic Reduction of Selenium Ions Using Different TiO2 Photocatalysts. Chem Eng Sci 60, 5759–5769, (2005), doi:10.1016/j.ces.2005.04.085.
27. Maver, K.; Arčon, I.; Fanetti, M.; Emin, S.; Valant, M.; Lavrenčič Štangar, U. Improved Photocatalytic Activity of Anatase-Rutile Nanocomposites Induced by Low-Temperature Sol-Gel Sn-Modification of TiO2. Catal Today 361, 124–129, (2021), doi:10.1016/j.cattod.2020.01.045.